PROCEEDINGS OF SCIENCE

Recent ATLAS Results

Martin Wessels[*†]
University of Heidelberg, Kirchhoff Institut for Physics
E-mail: martin.wessels@cern.ch

These proceedings review recent results of the ATLAS experiment at the Large Hadron collider LHC, using datasets corresponding to integrated luminosities of up to 4.9 fb^{-1}. The results reviewed here include measurements of the inclusive jet, W and Z boson cross sections, properties of top production such as the cross section and mass, and the observation of a new χ_b state. Latest results of searches for the Standard Model Higgs boson are also presented. Finally, searches for supersymmetry and other new physics models are discussed.

50th International Winter Meeting on Nuclear Physics - Bormio2012,
23-27 January 2012
Bormio, Italy

[*]Speaker.
[†]On behalf of the ATLAS Collaboration

PoS(Bormio2012)043

1. The ATLAS Detector

The ATLAS detector [1, 2] consists of an inner tracking system (inner detector, or ID) surrounded by a thin superconducting solenoid providing a 2 T magnetic field, electromagnetic and hadronic calorimeters, and a muon spectrometer (MS). The ID consists of pixel and silicon microstrip detectors, surrounded by a transition radiation tracker. The electromagnetic calorimeter is a liquid-argon and lead detector, split into barrel ($|\eta| < 1.475$) and endcap ($1.375 < |\eta| < 3.2$) regions. Hadron calorimetry is based on two different detector technologies. The barrel ($|\eta| < 0.8$) and extended barrel ($0.8 < |\eta| < 1.7$) calorimeters are composed of scintillator and steel, while the hadronic endcap calorimeters ($1.5 < |\eta| < 3.2$) utilize liquid-argon and copper. The forward calorimeters ($3.1 < |\eta| < 4.9$) are instrumented with liquid-argon/copper and liquid-argon/tungsten, providing electromagnetic and hadronic energy measurements, respectively. The MS is based on three large superconducting toroids arranged with an eight-fold azimuthal coil symmetry around the calorimeters, and a system of three stations of chambers for triggering and for precise track measurements.

2. Standard Model Measurements

2.1 Jet Physics

At the Large Hadron Collider jet production is the dominant high transverse-momentum (p_T) process. Jet cross sections serve as one of the main observables in high-energy particle physics, providing precise information on the structure of the proton. They are an important tool for understanding the strong interaction and searching for physics beyond the Standard Model (SM).

The ATLAS Collaboration has published a first measurement of inclusive jet and dijet production at $\sqrt{s} = 7$ TeV, using an integrated luminosity of 17 nb^{-1} [3]. The analysis presented in Reference [4] extends the previous measurement using the 2010 data sample of (37.3 ± 1.2) pb^{-1}, an integrated luminosity more than 2000 times larger than that of the previous study. This more than doubles the kinematic reach at high jet transverse momentum and large dijet invariant mass.

The inclusive jet double-differential cross section is shown in Figure 1 for jets reconstructed with the anti-k_t algorithm with $R = 0.4$. The measurement extends from jet transverse momentum of 20 GeV to almost 1.5 TeV, spanning two orders of magnitude in p_T and ten orders of magnitude in the value of the cross section. The results are compared to NLOJET++ predictions (using the CT10 PDF set) corrected for non-perturbative effects, where the theoretical uncertainties from scale variations, parton distribution functions, and non-perturbative corrections have been accounted for. Overall, the calculations agree with the data over many orders of magnitude, although the cross sections predicted by the theory tend to be larger than the measured values at large jet transverse momentum.

2.2 B Physics

Measurements of the properties of heavy quark-antiquark bound states, or quarkonia, provide a unique insight into the nature of Quantum Chromodynamics (QCD) close to the strong decay threshold. In the presented analysis [5], χ_b quarkonium states are reconstructed with the ATLAS detector through the radiative decay modes $\chi_b(n\mathrm{P}) \to \Upsilon(1\mathrm{S})\gamma$ and $\chi_b(n\mathrm{P}) \to \Upsilon(2\mathrm{S})\gamma$, in which

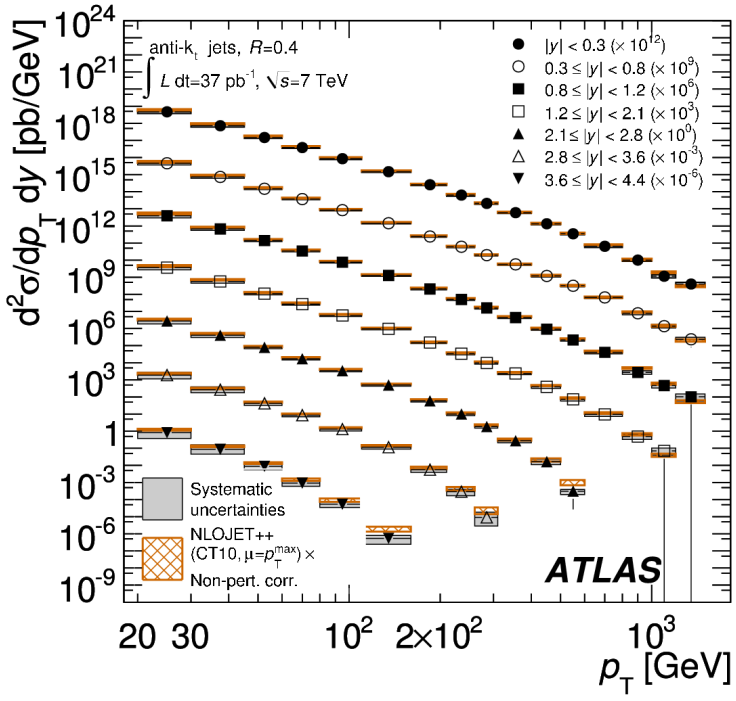

Figure 1: Inclusive jet double-differential cross section as a function of jet p_T in different regions of $|y|$ for jets identified using the anti-k_t algorithm with $R = 0.4$. For convenience, the cross sections are multiplied by the factors indicated in the legend.

$\Upsilon(1S,2S) \to \mu^+\mu^-$ and the photon is reconstructed either through conversion to e^+e^- or by direct calorimetric measurement.

The di-muon selection requires a pair of oppositely charged muons, which are fitted to a common vertex. The invariant mass distribution, $m_{\mu\mu}$, of di-muon candidates is shown in Figure 2. Those candidates with masses in the ranges $9.25 < m_{\mu\mu} < 9.65$ GeV and $9.80 < m_{\mu\mu} < 10.10$ GeV are selected as $\Upsilon(1S)$ and $\Upsilon(2S)$ candidates, respectively. The χ_b candidates are formed by associating a reconstructed $\Upsilon \to \mu^+\mu^-$ candidate with a reconstructed photon. The invariant mass difference $\Delta m = m(\mu^+\mu^-\gamma) - m(\mu^+\mu^-)$ is calculated to minimize the effect of $\Upsilon \to \mu^+\mu^-$ mass resolution. In order to compare the Δm distributions of both $\chi_b(n\mathrm{P}) \to \Upsilon(1\mathrm{S})\gamma$ and $\chi_b(n\mathrm{P}) \to \Upsilon(2\mathrm{S})\gamma$ decays, the variable $\tilde{m}_k = \Delta m + m_{\Upsilon(k\mathrm{S})}$ is defined, where $\Upsilon(k\mathrm{S})$ are the world average masses [6] of the $\Upsilon(k\mathrm{S})$ states.

Figure 3 shows the the $\tilde{m}_1$ and $\tilde{m}_2$ distributions for converted photons. In addition to the expected peaks for $\chi_b(1\mathrm{P},2\mathrm{P}) \to \Upsilon(1\mathrm{S},2\mathrm{S})\gamma$, structures are observed at an invariant mass of approximately 10.5 GeV. These additional structures are interpreted as the radiative decays of the previously unobserved $\chi_b(3\mathrm{P})$ states, $\chi_b(3\mathrm{P}) \to \Upsilon(1\mathrm{S})\gamma$ and $\chi_b(3\mathrm{P}) \to \Upsilon(2\mathrm{S})\gamma$. The mass barycenter for the $\chi_b(3\mathrm{P})$ signal, determined from the fit using converted photon candidates with a substantially smaller systematic uncertainty, is $\bar{m}_3 = 10.530 \pm 0.005(\mathrm{stat.}) \pm 0.009(\mathrm{syst.})$ GeV. The result is consistent with theoretical predictions; the current mass resolution of the measurement is of similar magnitude to the expected hyperfine splittings.

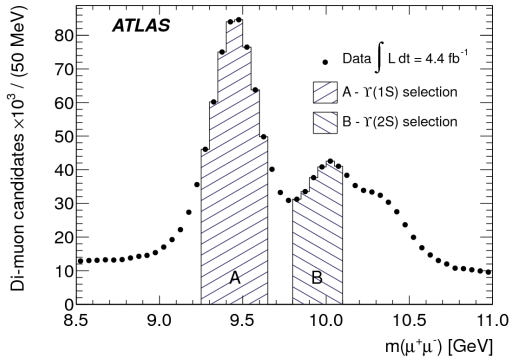

Figure 2: The invariant mass of selected di-muon candidates. The shaded regions *A* and *B* show the selections for $\Upsilon(1S)$ and $\Upsilon(2S)$ candidates respectively.

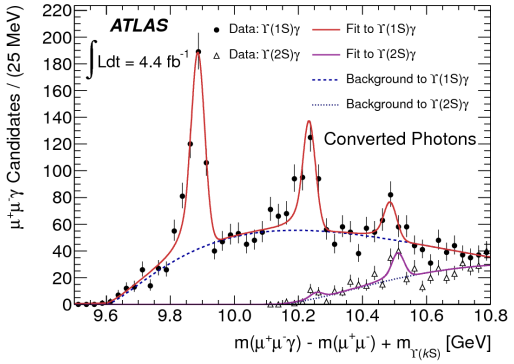

Figure 3: The mass distributions of $\chi_b \to \Upsilon(k\mathrm{S})\gamma$ ($k = 1,2$) candidates formed using converted photons. Data are shown before the correction for the energy loss from the photon conversion electrons due to bremsstrahlung and other processes. The data for decays of $\chi_b \to \Upsilon(1\mathrm{S})\gamma$ and $\chi_b \to \Upsilon(2\mathrm{S})\gamma$ are plotted using circles and triangles respectively. Solid lines represent the total fit result for each mass window. The dashed lines represent the background components only.

2.3 W and Z Production

The inclusive Drell-Yan production cross sections of W and Z bosons have been an important testing ground for QCD. The presented measurement [7] determines the cross sections times leptonic branching ratios, $\sigma_{W^\pm} \cdot BR(W \to l\nu)$ and $\sigma_{Z/\gamma^*} \cdot BR(Z/\gamma^* \to ll)$, of inclusive W and Z production for electron and muon final states, where $l = e, \mu$. The cross section values are integrated over the fiducial region of the analysis and also extrapolated to the full kinematic range. The data are also reported differentially, as functions of the lepton pseudorapidity η_l, for the $W^\pm$ cross sections, and of the boson rapidity, y_Z, for the Z/γ^* cross section. The electron and muon $W^\pm$ and Z cross sections are combined to form a single joint measurement taking into account the systematic error correlations between the various data sets.

The combined differential Z cross section is compared in Figure 4 with the calculated NNLO predictions using the JR09, ABKM09, HERAPDF1.5 and MSTW08 NNLO PDF sets. One observes that the measured y_Z dependency is broadly described by the predictions of the PDF sets considered. Some deviations, however, are visible, for example the lower Z cross section at central rapidities in the case of the JR09 PDF set, or the tendency of the ABKM09 prediction to overshoot the Z cross sections at larger y_Z. It thus can be expected that the differential cross sections presented here will reduce the uncertainties of PDF determinations and also influence the central values.

2.4 Di-Boson Production

The production of pairs of W and Z bosons at the LHC is of great interest since it provides an excellent opportunity to test the predictions of the electroweak sector of the Standard Model at the TeV energy scale; moreover it is major irreducible background to the search for the Higgs bo-

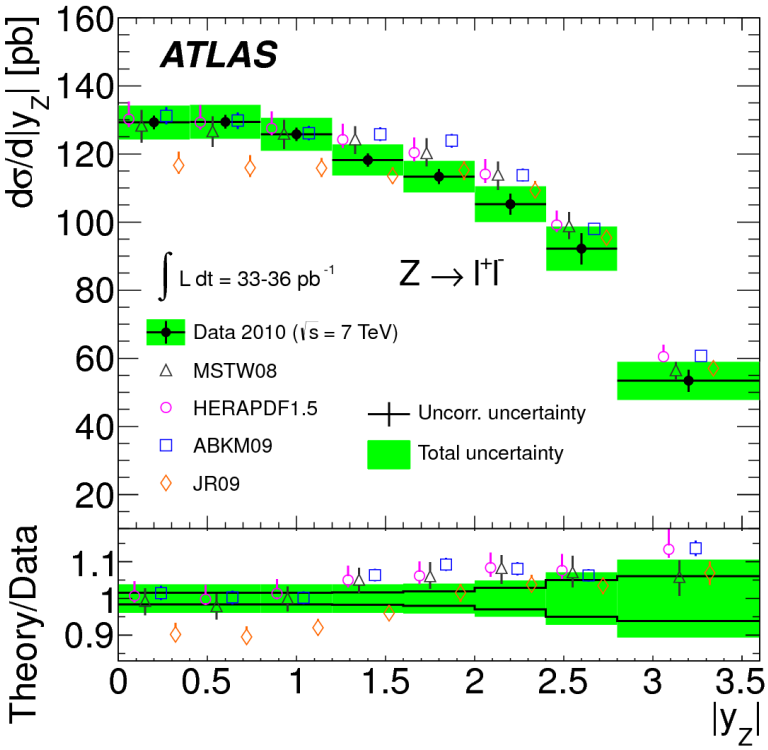

Figure 4: Differential $d\sigma/d|y_Z|$ cross section measurement for $Z \rightarrow ll$ compared to NNLO theory predictions using various PDF sets. The kinematic requirements are $66 < m_{ll} < 116$ GeV and $p_{T,l} > 20$ GeV. The ratio of theoretical predictions to data is also shown. Theoretical points are displaced for clarity within each bin.

son. ATLAS has recently published results measuring the W^+W^-, the $W^\pm Z$ and the ZZ production cross sections [8, 9, 10] using data corresponding to an integrated luminosity of 1.02 fb^{-1}. Doubly leptonic decay events are selected with electrons, muons and missing transverse momentum in the final states. All measurements of the cross sections are consistent with the Standard Model expectations. The invariant mass of the Z boson in $W^\pm Z$ candidate events is shown in Figure 5. A total of 71 $W^\pm Z$ candidates are observed in data, with $12.1 \pm 1.4(\text{stat.})^{+4.1}_{-2.0}(\text{syst.})$ expected background events. The invariant mass distribution of the combined four-lepton system for the selected ZZ candidates is shown in Figure 6. Twelve ZZ candidates are observed in data, with a background expectation of $0.3 \pm 0.3(\text{stat.})^{+0.4}_{-0.3}(\text{syst.})$.

2.5 Top Physics

The measurement of the top-quark pair-production cross section, σ_{SM}, is one of the key milestones for the early LHC physics program. A precise measurement of σ_{SM} allows precision tests of perturbative QCD, whose uncertainties on σ_{SM} are now at the level of 10% [11, 12]. In addition, $t\bar{t}$ production is an important background to the search for the Higgs boson and various searches for physics beyond the Standard Model. New physics may also give rise to additional $t\bar{t}$ production mechanisms or modification of the top quark decay channels.

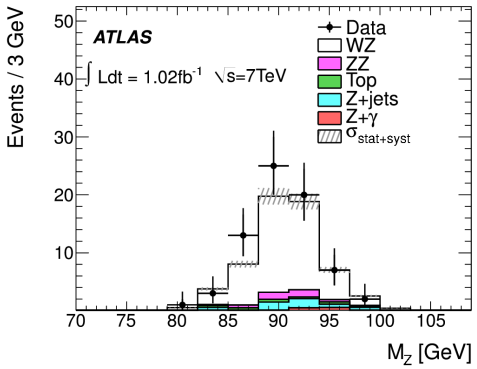

Figure 5: The invariant mass of the lepton pair attributed to the Z boson in candidate events after the full selection. The stacked histograms represent the predictions from simulation or, where applicable, data-driven estimates including the statistical and systematic uncertainty shown by shaded bands.

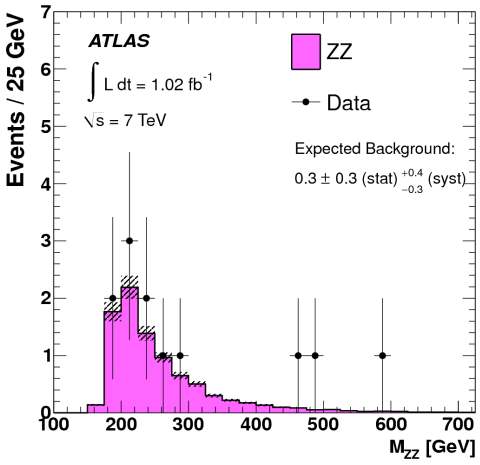

Figure 6: Invariant mass M_{ZZ} of the four-lepton system for the selected ZZ candidate events. The points represent the observed data and the histograms show the signal prediction from simulation. The shaded band on each histogram shows the combined statistical and systematic uncertainty on the signal prediction. The predicted number of background events from the data-driven background estimate is indicated on the plot.

Within the Standard Model, top quarks are predicted to decay to a W-boson and a b-quark ($t \to Wb$) nearly 100% of the time. Events with a $t\bar{t}$ pair can be classified as "single lepton", "dilepton", or "all hadronic" according to the decays of the two W-bosons: each can decay into quark-antiquark pairs ($W \to q_1 q_2$) or a lepton-neutrino pair ($W \to l\nu$).

Reference [13] presents a measurement of the top quark pair production cross section based on a statistical combination of measurements using dilepton final states with 0.70 fb^{-1} of data taken in 2011 [14] and single-lepton final states with 35 pb^{-1} of data taken in 2010 [13]. The measured cross section, which is in good agreement with the Standard Model prediction, is: $\sigma_{t\bar{t}} = 176 \pm 5(\text{stat.}) \pm^{13}_{10} (\text{syst.}) \pm 7(\text{lumi.})$ pb. Figure 7 shows various cross section measurements from Tevatron and the ATLAS experiment, overlaid on the theoretical predictions as a function of center-of-mass energy. The measurement presented in Reference [13], which has a total error of 8.2%, is approaching the precision of recent Tevatron cross section combinations, which measure 7.5 ± 0.48 pb at $\sqrt{s} = 1.96$ TeV for an error of 6.4% [15].

The top-quark mass is a fundamental parameter of the Standard Model of particle physics. Being about 40 times larger than the mass of its weak isospin partner, the b-quark, the top-quark mass gives large contributions to electroweak radiative corrections which, when connected to precision electroweak measurements, can be used to derive constraints on the masses of the Higgs boson and of heavy particles predicted by Standard Model extensions. The main methodology used to determine m_{top} at hadron colliders consists of measuring the invariant mass of the decay products

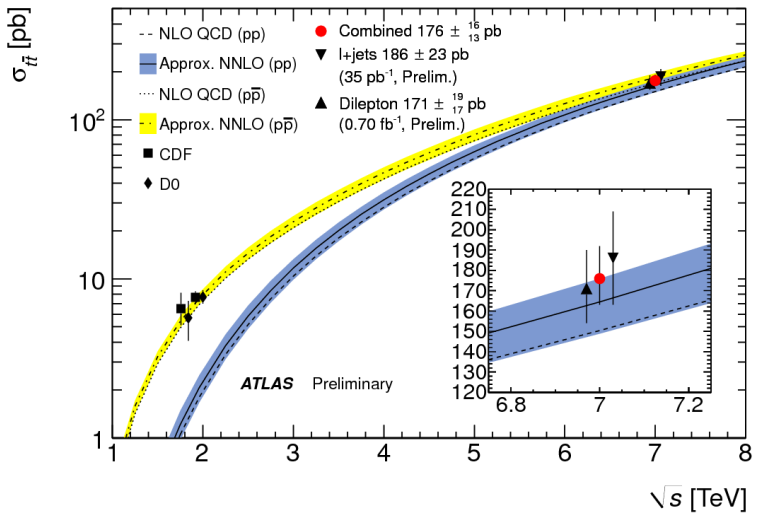

Figure 7: Dependence of $\sigma_{t\bar{t}}$ on $\sqrt{s}$ from theoretical predictions based on a top mass of 172.5 GeV together with the dilepton, single lepton, and combined measurements from ATLAS. Uncertainties on measurements are shown as vertical bars and include statistical, systematic, and luminosity contributions. Results obtained with the Tevatron are also shown. Measurements made at the same center-of-mass energy are slightly offset horizontally for clarity.

of the top-quark candidates and deducing m_{top} by using sophisticated analysis methods.

The most precise measurements of this type are based on the $t\bar{t}$ single-lepton channels. The top-quark mass has been measured directly via a 2-dimensional template method in both the electron and muon channels using data corresponding to an integrated luminosity of about 0.70 fb[1] [16]. Both channels lead to consistent results within their uncertainties. The uncertainty is dominated by the systematic uncertainties, where the main sources of uncertainty stem from the relative jet energy scale uncertainty. The results are shown in Figure 8, together with the most precise measurements from the Tevatron experiments [17].

The top quark holds great promise as a probe for new phenomena at the TeV scale. In Reference [18] a search for new phenomena in $t\bar{t}$ events with large missing transverse momentum in proton-proton collisions at a center-of-mass energy of 7 TeV is presented. The measurement is based on 1.04 fb[1] of data collected with the ATLAS detector at the LHC. The search is carried out in the single-lepton channel, characterized by an isolated lepton of high transverse momentum, four or more jets and large missing transverse momentum. Contributions to this final state may arise from a number of Standard Model extensions.

The E_T^{miss} distribution for data are shown in Figure 9 and compared with the background and signal predictions. The data are found to be consistent with Standard Model expectations. Using a model of pair-produced quark-like objects decaying to a top quark and a heavy neutral particle, a limit is established excluding masses of these top partners up to 420 GeV and stable weakly-interacting particle masses up to 140 GeV.

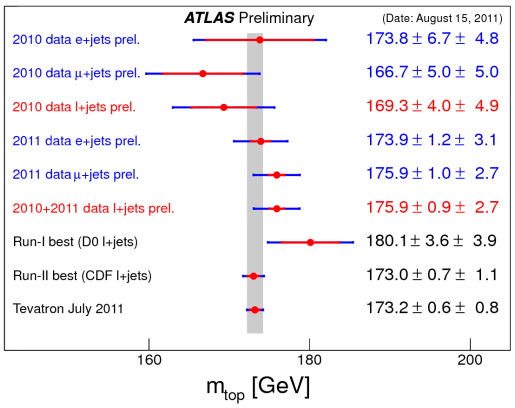

Figure 8: The results on m_{top} from the individual analyses and their combination compared to selected results from other measurements and to the present average value from the Tevatron experiments [17].

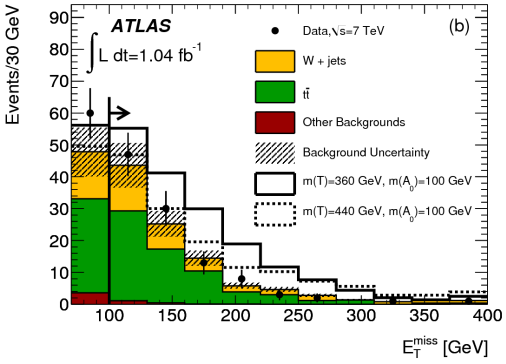

Figure 9: E_T^{miss} after applying all selection criteria except the cut on the variable shown. The line with the arrow indicates the selection criteria that defines the signal region ($E_T^{miss} > 100$ GeV). Expectations from two signal mass points are stacked separately on top of the SM background. The last bin includes the overflow.

3. Standard Model Higgs Searches

The search for the Standard Model Higgs boson is a major goal of the LHC program. Direct searches at the CERN LEP e^+e collider excluded at 95% confidence level (CL) the production of a Standard Model Higgs with $m_H < 114.4$ GeV [19]. The searches at the Fermilab Tevatron $p\bar{p}$ collider have excluded at 95% CL the region 156 GeV $< m_H <$ 177 GeV [20]. At the LHC, the latest results of the ATLAS Standard Model Higgs searches [21] based on data collected during the early part of the 2011 LHC run exclude the Higgs boson mass (m_H) ranges $146-230$ GeV, $256-282$ GeV and $296-459$ GeV at 95% CL, while for CMS the corresponding excluded ranges are $145-216$ GeV, $226-288$ GeV and $310-400$ GeV [22]. A preliminary combination of $1.0-2.3$ fb^1 of LHC data per experiment exclude the Standard Model Higgs in the region 141 GeV $< m_H <$ 476 GeV at 95% CL [23]. In ATLAS several final states are used to search for the Standard Model Higgs boson.

3.1 Diphoton Decay Channel

The diphoton decay mode is one of the most important channels in the search for the Standard Model Higgs boson in the low mass region in which the Standard Model Higgs boson is not yet excluded. Despite the low branching ratio ($\approx 0.2\%$), this channel provides good experimental sensitivity in the mass region below 150 GeV. In Reference [24] results are presented based on an integrated luminosity of 4.9 fb^{-1}, corresponding to the total proton-proton collision data sample recorded with the ATLAS detector in 2011.

The data analysis proceeds by selecting photon pairs with tight identification and isolation cuts to minimize backgrounds other than direct diphoton production. A narrow peak in the reconstructed invariant mass distribution is searched for over a large, smooth background, fitted with an exponential function with free slope and normalization parameters. The diphoton invariant mass

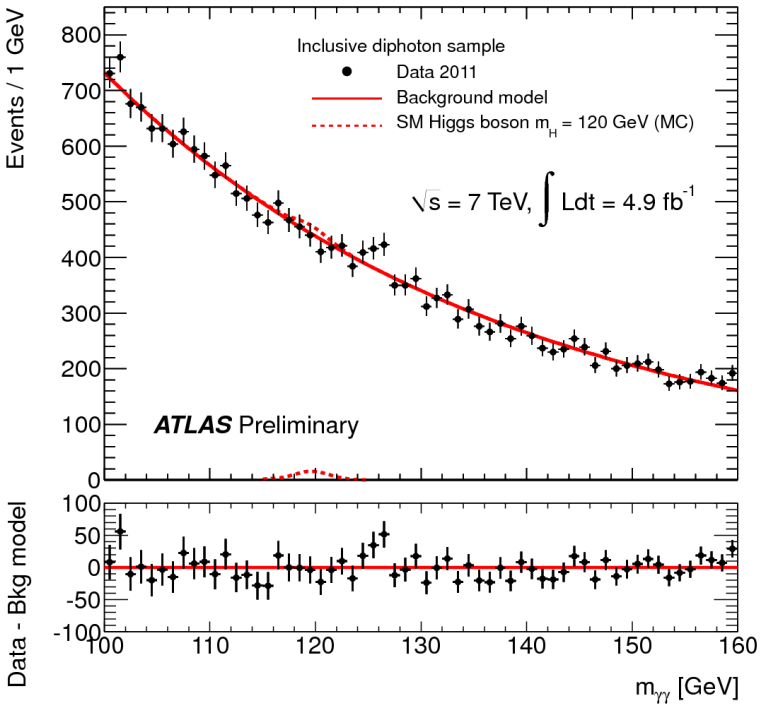

Figure 10: Diphoton invariant mass distribution, overlaid with the sum of the background-only fits and the signal expectation for a mass hypothesis of 120 GeV corresponding to the SM cross section. The figure below displays the residual of the data with respect to the background-only fit sum.

distribution ($m_{\gamma\gamma}$) is shown in Figure 10 (top) for the 22489 events passing the selection in the mass region 100 GeV $< m_{\gamma\gamma} <$ 160 GeV. Figure 10 (bottom) shows the residual of the data with respect to the sum of the background-only fits as a function of $m_{\gamma\gamma}$.

The statistical interpretation of the data follows the procedure described in [23] which adopts a modified frequentist approach (CL_S) for setting the limit and a frequentist approach to calculate the p_0-value. The p_0-value, used to quantify the probability of seeing an excess at least as large as the observed excess in the background-only hypothesis, is evaluated for Higgs boson mass hypotheses between 110 GeV and 150 GeV in steps of 1 GeV. The expected and observed p_0-values are shown in Figure 11. The minimal observed p_0-value is 0.27% and is found for a mass hypothesis of $m_H = 126$ GeV; this p_0-value corresponds to 2.8 standard deviations. The probability of such an excess appearing anywhere in the mass range investigated due to a background fluctuation, accounting for the look-elsewhere effect, is estimated to be approximately 7% and it reduces the observed significance to 1.5 standard deviations. The 95% confidence level limits on the ratio of the inclusive production cross section of a SM-like Higgs boson relative to the Standard Model cross section are also derived as shown in Figure 12.

3.2 The Decay Channel H $\rightarrow$ ZZ$^{(*)}$ $\rightarrow$ 4l

The search for the Standard Model Higgs through the decay $H \rightarrow ZZ^{(*)} \rightarrow l^+l^-l^+l^-$, where $l, l' = e, \mu$ provides good sensitivity in a wide mass range. Reference [25] presents an update of the

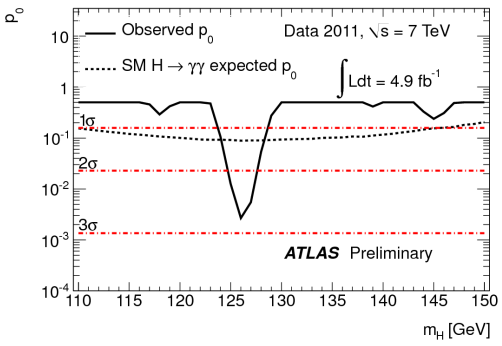

Figure 11: The observed and expected p_0-value as a function of the hypothesized Higgs boson mass without taking the look-elsewhere effect into account. The dotted-dashed lines indicate the corresponding significance.

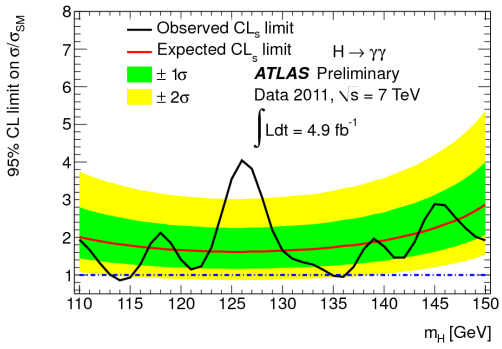

Figure 12: The observed and expected 95% confidence level limits, normalized to the SM Higgs boson cross sections, as a function of the hypothesized Higgs boson mass.

ATLAS search for a Standard Model Higgs boson in this channel for the mass range from 110 GeV to 600 GeV, using an average integrated luminosity of 4.8 fb^{-1}. Three distinct final states, $\mu\mu\mu\mu$ (4μ), $ee\mu\mu$ ($2e2\mu$), and $eeee$ ($4e$), are selected. The largest background to this search comes from continuum $ZZ^{(*)}$ production. For $m_H < 180$ GeV, contributions from Z+jets and $t\bar{t}$ processes, where the additional charged leptons arise either from decays of hadrons with heavy (b and c-quark) flavor content or from light-flavor-jets misidentified as leptons, are important.

In total 71 candidate events are selected by the analysis: 24 4μ, 30 $2e2\mu$, and 17 $4e$ events, while in the same mass range 62 ± 9 events are expected from the background processes; 18.6 ± 2.8 4μ, 29.7 ± 4.5 $2e2\mu$ and 13.4 ± 2.0 $4e$. The m_{4l} distribution for the total background and several signal hypotheses is compared to the data in Figure 13.

Upper limits are set on the Higgs boson production cross section at 95% CL, using the CLs modified frequentist formalism with the profile likelihood test statistic. The test statistic is evaluated with a maximum likelihood fit of signal and background models to the observed m_{4l} distribution. Figure 14 shows the expected and observed 95% CL cross section upper limits as a function of m_H. The most significant deviations from the background-only hypothesis are observed for $m_H = 125$ GeV with a local p_0-value of 1.8% (2.1σ), $m_H = 244$ GeV with a local p_0-value of 1.1% (2.3σ) and $m_H = 500$ GeV with a p_0-value of 1.4% (2.2σ). Once the look-elsewhere effect is considered, none of the observed local excesses is significant by itself.

3.3 Higgs Combinations

The results of a preliminary combination of Standard Model Higgs searches with the ATLAS experiment, in a dataset corresponding to an integrated luminosity of up to 4.9 fb^{-1} are presented in Reference [26]. The combination, in terms of the observed and the expected upper limit at the 95% CL on the Higgs boson production cross section, normalized to the Standard Model value, of all channels is shown in Figure 15. The Higgs boson mass ranges from 112.7 GeV to 115.5 GeV, 131 GeV to 237 GeV and 251 GeV to 468 GeV are excluded at the 95% CL, while the expected Higgs boson mass exclusion in the absence of a signal ranges from 124.6 GeV to 520 GeV. An

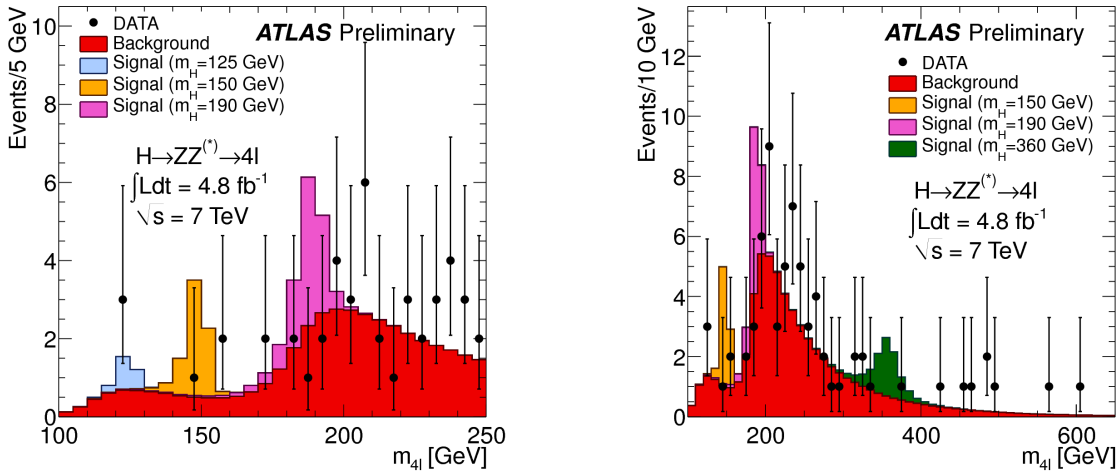

Figure 13: m_{4l} distribution of the selected candidates, compared to the background expectation. Error bars represent 68.3% central confidence intervals. The signal expectation for several m_H hypotheses is also shown. The resolution of the reconstructed Higgs mass is dominated by detector resolution at low m_H values and by the Higgs boson width at high m_H.

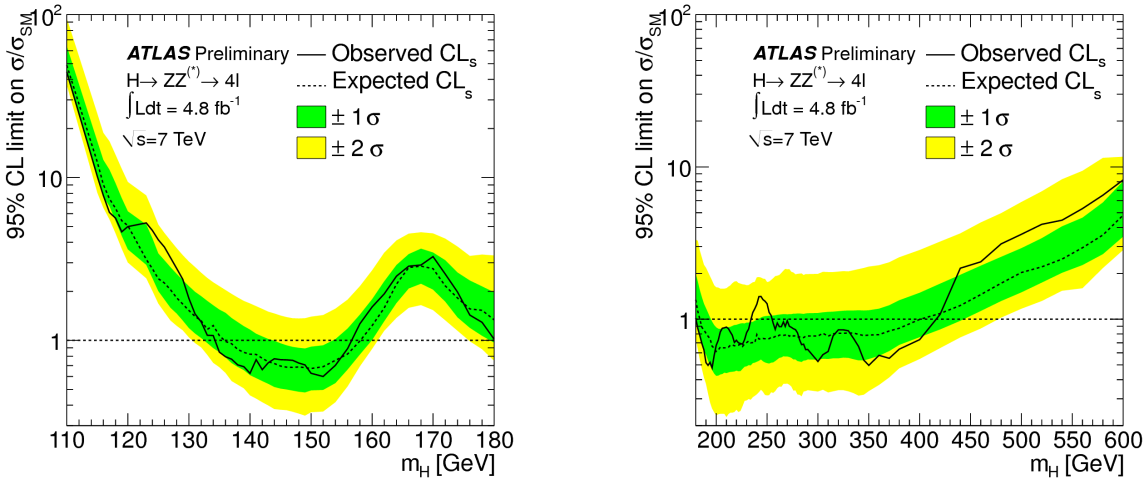

Figure 14: The expected (dashed) and observed (full line) 95% CL upper limits on the Higgs boson production cross section as a function of the Higgs boson mass, divided by the expected SM Higgs boson cross section. The green and yellow bands indicate the expected sensitivity with $\pm 1\sigma$ and $\pm 2\sigma$ fluctuations, respectively.

excess of events is observed for a Higgs boson mass hypothesis close to $m_H = 126$ GeV. As depicted in Figure 16, the maximum local significance of this excess is 3.6σ above the expected Standard Model background, while the global probability of such a fluctuation to happen anywhere in the full explored Higgs mass domain is estimated to be approximately 1%, corresponding to a global significance of 2.3σ.

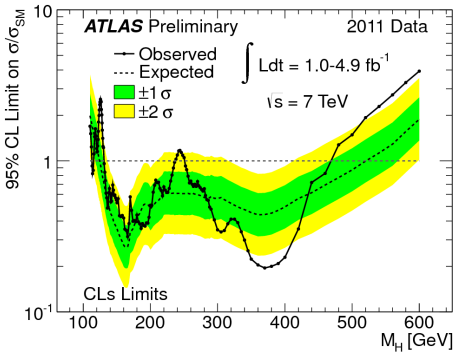

Figure 15: The combined upper limit on the Standard Model Higgs boson production cross section divided by the Standard Model expectation as a function of m_H is indicated by the solid curve. The dotted curve shows the median expected limit in the absence of a signal and the green and yellow bands indicate the corresponding 68% and 95% expected regions.

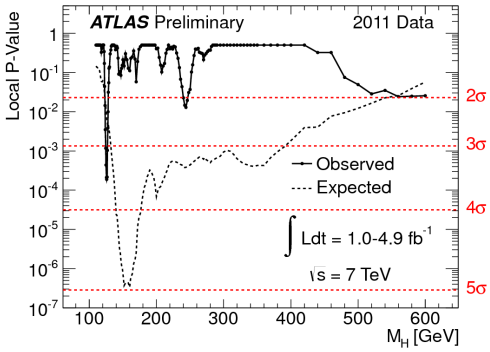

Figure 16: The consistency of the observed results with the background-only hypothesis is shown in the full mass range of the analysis. The dashed curve show the median expected significance in the hypothesis of a Standard Model Higgs boson production signal.

4. Beyond the Standard Model Searches

4.1 Supersymmetry

Many extensions of the Standard Model include heavy colored particles, some of which could be accessible at the LHC. The squarks and gluinos of supersymmetric (SUSY) theories are one class of such particles. In Reference [27] a search for squarks and gluinos in final states containing only jets and large missing transverse momentum is presented. This final state can be generated by a large number of R-parity conserving models [28, 29] in which squarks, $\tilde{q}$, and gluinos, $\tilde{g}$, can be produced in pairs $\{\tilde{g}\tilde{g}, \tilde{q}\tilde{q}, \tilde{q}\tilde{g}\}$ and can decay via $\tilde{q} \to q\tilde{\chi}_1^0$ and $\tilde{g} \to q\bar{q}\tilde{\chi}_1^0$ to weakly interacting neutralinos, $\tilde{\chi}_1^0$, which escape the detector unseen. Processes contributing to $\tilde{g}\tilde{g}$, $\tilde{q}\tilde{q}$ and $\tilde{q}\tilde{g}$ final states lead to events containing at least two, three or four jets, respectively. Cascade decays of heavy particles tend to increase the final state multiplicity.

In order to achieve maximal reach over the $(m_{\tilde{g}}, m_{\tilde{q}})$-plane, five signal regions are defined, characterized by increasing jet multiplicity requirements and high effective mass, m_{eff}, which is calculated as the sum of E_T^{miss} and the magnitudes of the transverse momenta of the two, three or four highest p_T jets used to define the signal region. Data recorded by the ATLAS experiment at the LHC corresponding to an integrated luminosity of 1.04 fb[1] have been used. Good agreement is seen between the numbers of events observed in the five signal regions and the numbers of events expected from Standard Model sources. Figure 17 shows the observed m_{eff} distribution in the signal region for the four-jet high-mass channel together with Monte Carlo background expectations.

The exclusion limits placed on non-SM cross sections impose new constraints on scenarios with novel physics. Data from the five signal regions are used to set the limits, taking the signal region with the best expected limit at each point in parameter space. Gluino and squark masses below

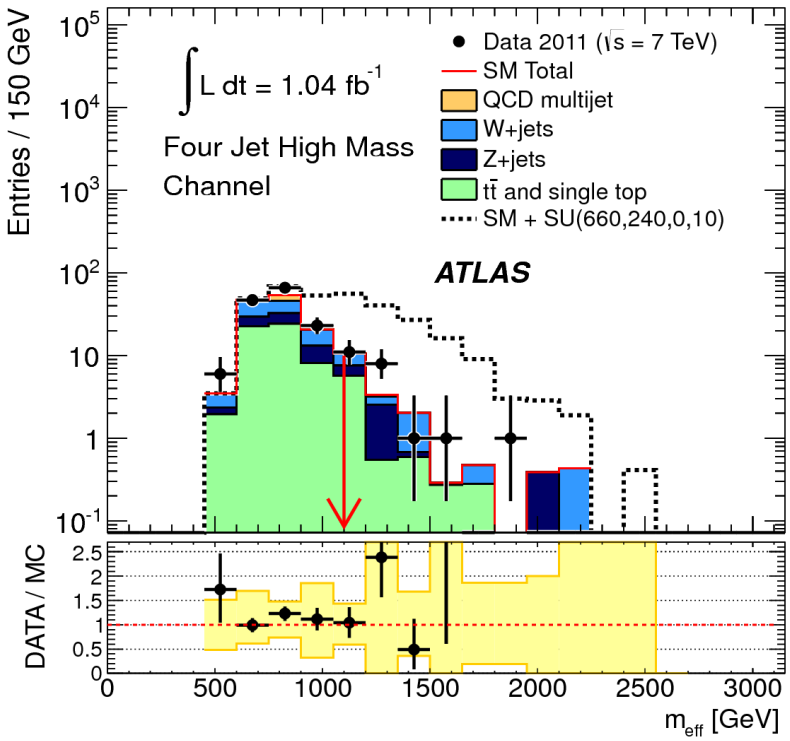

Figure 17: The observed m_{eff} distribution in the signal region for the four-jet high-mass channel using the inclusive definition of m_{eff}, after all the selection criteria but the m_{eff} cut. These plots also show the expected SM contributions obtained from Monte Carlo simulated samples. The red arrows indicate the lower bounds on m_{eff} used in the final signal region selections. The expectation for a specific MSUGRA/CMSSM reference point is also shown. In the lower figure the ratio of the data to the SM expectation is provided. Black vertical bars show the statistical uncertainty from the data, while the yellow band shows the size of the systematic uncertainties from the Monte Carlo simulation.

700 GeV and 875 GeV respectively are excluded at the 95% confidence level in simplified models containing only squarks of the first two generations, a gluino octet and a massless neutralino.

The search for supersymmetry at ATLAS is carried out using many different selection criteria in order to maximize overall sensitivity. The mass reach of a representative selection of ATLAS searches for supersymmetry is shown in Figure 18.

4.2 Beyond Supersymmetry

The Standard Model is an extremely successful effective theory which has been extensively tested over the past forty years. However, a number of fundamental questions are left unanswered. In particular, the Standard Model does not provide an explanation for the source of the mass hierarchy and the generational structure of quarks and leptons. Compositeness models address these questions by proposing that quarks and leptons are composed of hypothetical constituents named preons. New interactions among quarks and leptons should then be visible at the scale of the constituents' binding energies, and give rise to excited states.

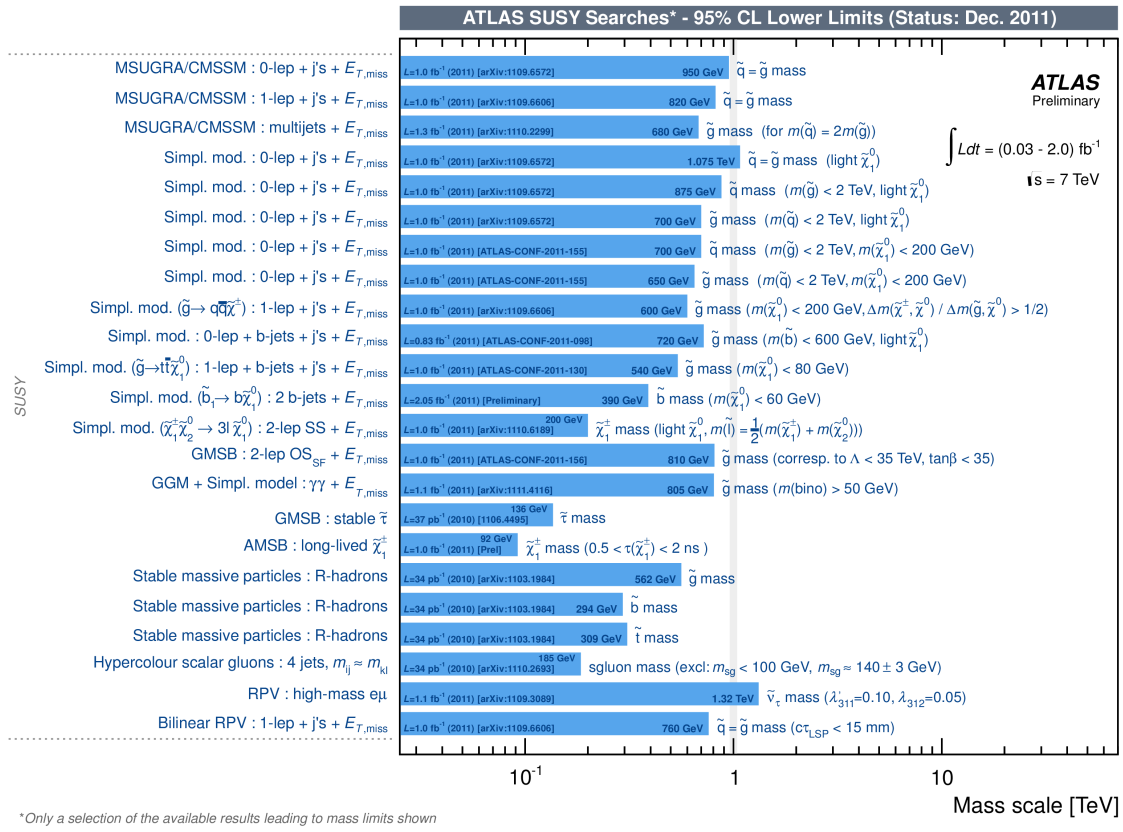

Figure 18: Mass reach of ATLAS searches for supersymmetry. Only a representative selection of the available results is shown.

In Reference [32] a search for excited electrons and muons in the $l^* \to l\gamma$ channel based on 2.05 fb^{-1} data is reported. In the benchmark signal model considered [33], excited leptons may be produced singly via $q\bar{q} \to l^*\bar{l}$ or in pairs via $q\bar{q} \to l^*\bar{l}^*$, due to contact interactions. As the cross section for pair production is much less than for single production, the search for excited leptons is based on the search for events with $l\bar{l}\gamma$ in the final state: three very energetic particles, isolated, and well separated from one another.

The signature of excited leptons can present itself as a peak in the $l\bar{l}\gamma$ invariant mass ($m_{ll\gamma}$) spectrum, which is presented in Figure 19 for the e^* channel. The observed invariant mass spectra are consistent with Standard Model background expectations. Limits are set on the cross section times branching ratio $\sigma B(l^* \to l\gamma)$ at 95% confidence limit. The limits are translated into bounds on the compositeness scale Λ as a function of the mass of the excited leptons and are the most stringent bounds to date on excited leptons for the parameter-space region with $m_{l^*} > 200$ GeV.

Similarities between leptons and quarks in the Standard Model suggest that they might be a part of some symmetry at energy scales above the electroweak symmetry breaking scale. In this type of symmetry, transitions between leptons and quarks, mediated by a new type of gauge boson,

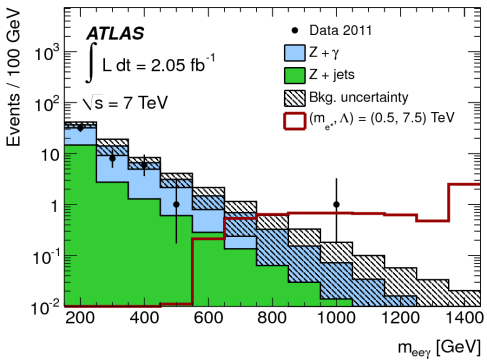

Figure 19: The invariant mass distribution for the $ll\gamma$ system for the e^* channel. The expected background uncertainties shown correspond to the sum in quadrature of the statistical uncertainties as well as the uncertainty in the Z + jets normalization measured in the control region. One event lies outside the mass range shown.

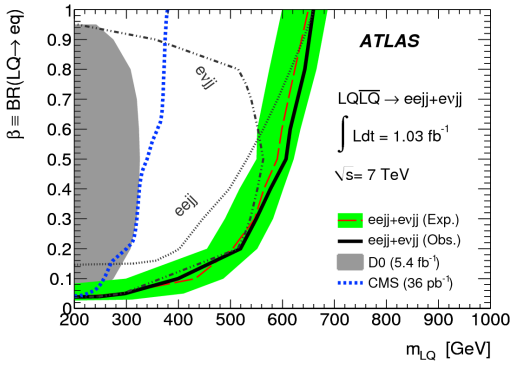

Figure 20: 95% CL exclusion region resulting from the combination of the two channels shown in the β versus leptoquark mass plane. The shaded area indicates the D0 exclusion limit [30], while the thick dotted line indicates the CMS exclusion [31]. The dotted and dotted-dashed lines indicate the individual limits for the $eejj$ and the $e\nu jj$, respectively. The combined observed limit is indicated by the solid black line.

a leptoquark (LQ), may occur. LQs are putative color-triplet bosons with spin 0 or 1, and fractional electric charge. They are predicted in many extensions of the Standard Model, such as Grand Unification models, and possess both quark and lepton quantum numbers. It is usually assumed that leptoquarks only couple to one generation of Standard Model isospin multiplet; consequently they are classified as first-, second-, or third-generation according to the fermion generation to which they couple.

Reference [34] presents the results of a search for the pair production of first generation scalar leptoquarks, using data corresponding to an integrated luminosity of 1.03 fb^{-1}. The search is performed in two different final states. In the first one both LQs decay into an electron and a quark, while in the second final state one of the LQs decays into an electron and a quark and the other LQ decays into an electron-neutrino and a quark; these result in two different experimental signatures.

No excess over Standard Model background expectations is observed in the data in the signal enhanced region and 95% CL upper bounds on the production cross section are thus determined. The obtained limits are combined and reinterpreted as limits in the β vs. m_{LQ} plane as shown in Figure 20, where β is the LQ's branching fraction to a charged lepton. Lower observed (expected) limits on leptoquark masses of $m > 660(650)$ GeV and $m > 607(587)$ GeV are obtained when assuming β to be equal to 1.0 and 0.5, respectively. These are the most stringent limits to date arising from direct searches for leptoquarks.

References

[1] The ATLAS Collaboration. The ATLAS Experiment at the CERN Large Hadron Collider. *Journal of Instrumentation*, 3(08):S08003, 2008.

[2] The ATLAS Collaboration. Expected Performance of the ATLAS Experiment - Detector, Trigger and Physics. 2009.

[3] The ATLAS Collaboration. Measurement of inclusive jet and dijet cross sections in proton-proton collisions at 7 TeV centre-of-mass energy with the ATLAS detector. *The European Physical Journal C - Particles and Fields*, 71:1–59, 2011.

[4] The ATLAS Collaboration. Measurement of inclusive jet and dijet production in pp collisions at $\sqrt{s} = 7$ TeV using the ATLAS detector. CERN-PH-EP-2011-192, 2011.

[5] The ATLAS Collaboration. Observation of a new χ_b state in radiative transitions to $\Upsilon(1S)$ and $\Upsilon(2S)$ at ATLAS. CERN-PH-EP-2011-225, 2011.

[6] K Nakamura and Particle Data Group. Review of Particle Physics. *Journal of Physics G: Nuclear and Particle Physics*, 37(7A):075021, 2010.

[7] The ATLAS Collaboration. Measurement of the inclusive $W^{\pm}$ and Z/γ cross sections in the electron and muon decay channels in pp collisions at $\sqrt{s} = 7$ TeV with the ATLAS detector. CERN-PH-EP-2011-143, 2011.

[8] The ATLAS Collaboration. Measurement of the WW cross section in $\sqrt{s} = 7$ TeV pp collisions with the ATLAS detector and limits on anomalous gauge couplings. CERN-PH-EP-2012-060, 2012.

[9] The ATLAS Collaboration. Measurement of the WZ production cross section and limits on anomalous triple gauge couplings in proton-proton collisions at $\sqrt{s} = 7$ TeV with the ATLAS detector. *Phys.Lett.*, B709:341–357, 2012.

[10] The ATLAS Collaboration. Measurement of the ZZ production cross section and limits on anomalous neutral triple gauge couplings in proton-proton collisions at $\sqrt{s} = 7$ TeV with the ATLAS detector. *Phys.Rev.Lett.*, 108:041804, 2012.

[11] Sven Moch and Peter Uwer. Theoretical status and prospects for top-quark pair production at hadron colliders. *Phys.Rev.*, D78:034003, 2008.

[12] U. Langenfeld, S. Moch, and P. Uwer. New results for t anti-t production at hadron colliders. DESY-09-104, SFB-CPP-09-61, HU-EP-09-31, 2009.

[13] The ATLAS Collaboration. Measurement of the top quark pair production cross-section based on a statistical combination of measurements of dilepton and single-lepton final states at $\sqrt{s} =$ 7 TeV with the ATLAS detector. ATLAS-CONF-2011-108, Aug 2011.

[14] The ATLAS Collaboration. Measurement of the top quark-pair cross-section with ATLAS in pp collisions at $\sqrt{s} = 7$ TeV in the single-lepton channel using b-tagging. ATLAS-CONF-2011-035, Mar 2011.

[15] The CDF Collaboration. Combination of CDF top quark pair production cross-section measurements with up to 4.6 fb-1. Conf Note 9913, 2009.

[16] The ATLAS Collaboration. Measurement of the top quark mass from 2011 ATLAS data using the template method. ATLAS-CONF-2011-120, Aug 2011.

[17] The CDF and D0 Collaboration. Combination of CDF and D0 results on the mass of the top quark using up to 5.8 fb^{-1} of data. FERMILAB-TM-2504-E, CDF-NOTE-10549, D0-NOTE-6222, 2011.

[18] The ATLAS Collaboration. Search for New Phenomena in ttbar Events With Large Missing Transverse Momentum in Proton-Proton Collisions at $\sqrt{s} = 7$ TeV with the ATLAS Detector. *Phys.Rev.Lett.*, 108:041805, 2012.

[19] R. Barate et al. Search for the standard model Higgs boson at LEP. *Phys.Lett.*, B565:61–75, 2003.

[20] The CDF and D0 Collaborations. Combined CDF and D0 Upper Limits on Standard Model Higgs Boson Production with up to 8.6 fb^{-1} of Data. FERMILAB-CONF-11-354-E, 2011.

[21] The ATLAS Collaboration. Update of the Combination of Higgs Boson Searches in pp Collisions at $\sqrt{s} = 7$ TeV with the ATLAS Experiment at the LHC. ATLAS-CONF-2011-135, Sep 2011.

[22] The CMS Collaboration. Search for standard model Higgs boson in pp collisions at $\sqrt{s} = 7$ TeV and integrated luminosity up to 1.7 fb-1. CMS-PAS-HIG-11-022, 2011.

[23] The ATLAS and CMS Collaborations. Combined Standard Model Higgs boson searches with up to 2.3 fb^{-1} of pp collisions at $\sqrt{s} = 7$ TeV at the LHC. ATLAS-CONF-2011-157, CMS-PAS-HIG-11-023, Nov 2011.

[24] The ATLAS Collaboration. Search for the Standard Model Higgs boson in the diphoton decay channel with 4.9 fb-1 of ATLAS data at $\sqrt{s} = 7$ TeV. ATLAS-CONF-2011-161, Dec 2011.

[25] The ATLAS Collaboration. Search for the Standard Model Higgs boson in the decay channel $H \to ZZ^{(*)} \to 4\ell$ with 4.8 fb^{-1} of pp collisions at $\sqrt{s} = 7$ TeV. ATLAS-CONF-2011-162, Dec 2011.

[26] The ATLAS Collaboration. Combination of Higgs Boson Searches with up to 4.9 fb^{-1} of pp Collisions Data Taken at a center-of-mass energy of 7 TeV with the ATLAS Experiment at the LHC. ATLAS-CONF-2011-163, Dec 2011.

[27] The ATLAS Collaboration. Search for squarks and gluinos using final states with jets and missing transverse momentum with the ATLAS detector in $\sqrt{s} = 7$ TeV proton-proton collisions. *Phys.Lett.*, B710:67–85, 2012.

[28] P. Fayet. Spontaneously broken supersymmetric theories of weak, electromagnetic and strong interactions. *Physics Letters B*, 69(4):489 – 494, 1977.

[29] Glennys R. Farrar and Pierre Fayet. Phenomenology of the production, decay, and detection of new hadronic states associated with supersymmetry. *Physics Letters B*, 76(5):575 – 579, 1978.

[30] The D0 Collaboration. Search for first generation leptoquark pair production in the electron + missing energy + jets final state. *Phys. Rev. D*, 84:071104, Oct 2011.

[31] The CMS Collaboration. Search for first generation scalar leptoquarks in the channel in pp collisions at $\sqrt{s} = 7$ TeV. *Physics Letters B*, 703(3):246 – 266, 2011.

[32] The ATLAS Collaboration. Search for excited leptons in proton-proton collisions at $\sqrt{s} = 7$ TeV with the ATLAS detector. CERN-PH-EP-2011-224, 2012.

[33] U. Baur, M. Spira, and P. M. Zerwas. Excited quark and lepton production at hadron colliders. *Phys. Rev. D*, 42:815–824, Aug 1990.

[34] The ATLAS Collaboration. Search for first generation scalar leptoquarks in pp collisions at $\sqrt{s} = 7$ TeV with the ATLAS detector. *Phys.Lett.*, B709:158–176, 2012.